On-chip biasing of the common-gate stages in the cascodes is provided by connecting their gates to the forward voltage of a Schottky diode. The current density through these stages is designed so that the V_{gs} is sufficiently negative to maintain the previous devices, M_1 and M_8, in saturation. On-chip decoupling capacitors are used at the gates of the cascode devices.

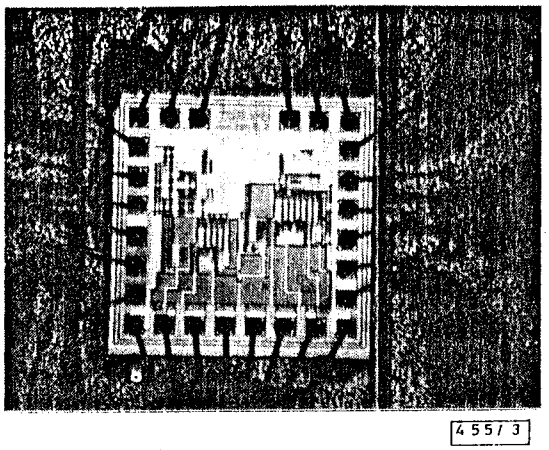

Fig. 3 *Die photograph of GaAs IC amplifier mounted in microwave package*

Experimental results: The amplifier (Fig. 3) was fabricated as part of a multiproject chip reticle at TriQuint Semiconductor using a depletion-mode GaAs MESFET process. Table 1 summarises the characteristics of this technology. The measured insertion gain of the amplifier (Fig. 4) indicates a DC gain of 26 dB and a −3 dB bandwidth of 3·2 GHz in good agreement with the simulated response. The input and output VSWR (Fig. 4) are less than 2·5 : 1 over the passband. The measured noise figure (Fig. 5) is between 5·5 dB and 6·5 dB over the midband range of frequencies. The amplifier exhibits a saturated output power of 10 dBm and an output power of 8 dBm at the −1 dB gain compression point. Nominal power dissipation for the circuit is 850 mW. The measured performance of the amplifier is summarised in Table 2.

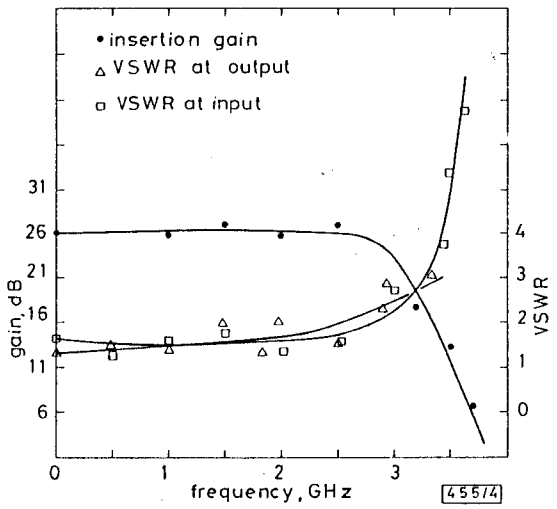

Fig. 4 *Measured performance of amplifier*

Insertion gain, VSWR at input terminal and VSWR at output terminal

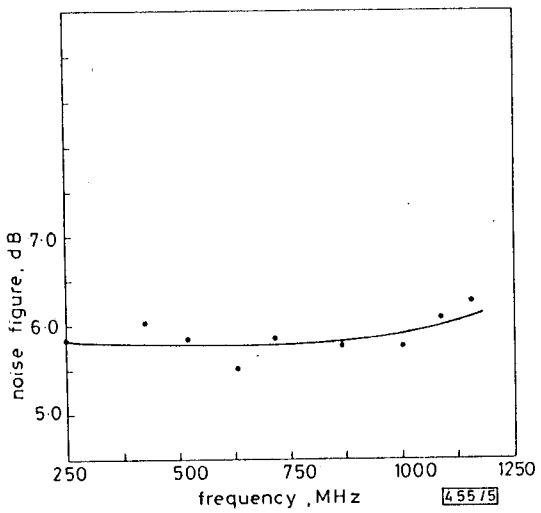

Fig. 5 *Measured noise figure of amplifier*

Table 1 TYPICAL MESFET PARAMETERS FOR $W = 300\,\mu m$, $L = 1\,\mu m$

I_{DSS}	42 mA
V_P	−1·5 V
g_m	40 mS
C_{gs}	475 fF
C_{gd}	40 fF
C_{ds}	75 fF
R_{ds}	450 Ω
f_T	13 GHz

Table 2 AMPLIFIER PERFORMANCE

Gain	26 dB
Bandwidth	3·2 GHz
Worst input VSWR	2·5 : 1
Worst output VSWR	2·5 : 1
Noise figure	6·5 dB
$P_{-1\,dB}$	8 dBm
Saturation power	10 dBm
Power dissipation	850 mW
Die size	1 mm × 1 mm

Acknowledgment: This research is supported by the State of California MICRO Program and TriQuint Semiconductor.

W. T. COLLERAN
A. A. ABIDI

Integrated Circuits & Systems Laboratory
Electrical Engineering Department
University of California
Los Angeles, CA 90024, USA

27th May 1987

References

1 KUKIELKA, J., and SNAPP, C.: 'Wideband monolithic cascadable feedback amplifiers using silicon bipolar technology'. IEEE microwave and millimeter wave monolithic IC symposium, 1982
2 MEYER, R. G., and BLAUSCHILD, R. A.: 'A four terminal wideband monolithic amplifier'. ISSCC digest of technical papers, New York, 1981, pp. 186–187
3 MANZ, B.: 'DC to 2·5 GHz MMIC amp focuses on fiber optics', *RF & Microwaves*, Feb. 1986, pp. 123–125
4 HORNBUCKLE, D. P., and VAN TUYL, R. L.: 'Monolithic GaAs direct coupled amplifiers', *IEEE Trans.*, 1981, **ED-28**, pp. 175–182

NONLINEAR VIBRATIONS AND HYSTERESIS OF MICROMACHINED SILICON RESONATORS DESIGNED AS FREQUENCY-OUT SENSORS

Indexing terms: Resonators, Optical sensors

Experimental observation of nonlinear vibrations and hysteresis of micromachined silicon resonators is reported. The experimental results are explained using a simple model in which the restoring force acting in the resonator contains a small cubic term. The effects will impose a limit to the maximum amplitude which can be excited while still maintaining reliability of these devices as frequency-out sensors.

Introduction: Sensor applications of micromachined silicon mechanical resonators are of great interest because of their frequency output,[1] and to avoid any electromagnetic interference it is desirable to have both optical activation and

optical interrogation. Interferometric displacement detection systems provide the necessary sensitivity to deal with an amplitude of vibration as small as a few nanometres, but these systems may require special compensation or isolation techniques to avoid any perturbation induced by the environment. These difficulties can be reduced significantly by using a non-interferometric technique for interrogation,[2] and this has the added advantage that multimode fibre and low-coherence sources can be used. However, such systems are less sensitive and will require the excitation of relatively large amplitudes of the silicon mechanical resonator, i.e. of the order of micrometres.

We report in this letter the observation of a nonlinear response, and hysteresis, of micromachined silicon resonators when large amplitudes of vibration are excited. This can clearly limit the application of the noninterferometric system for interrogation.

Measurements have been made on a number of micromachined silicon resonators of different geometries, a simple beam, a double-ended tuning fork and a coupled pair of suspended rectangular plates. The results shown here refer to this last device since its higher Q-factor makes it easier to obtain accurate measurements of its characteristics, but the same qualitative behaviour has been observed in the others.

Experimental arrangement: Fig. 1 shows a diagram of the resonator and its holder. The device which includes this resonator is designed as a pressure transducer and is fully described elsewhere.[3]

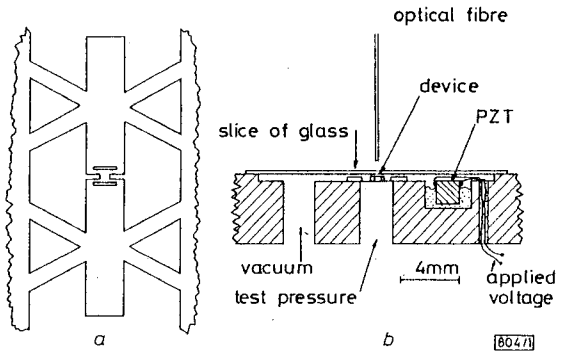

Fig. 1

a Diagram of resonator, 8 μm thickness
b Device holder

Piezoelectric excitation is used to be able to excite large amplitudes of vibration and the device is mounted in a vacuum to increase the Q-factor of the resonator. A single-mode optical fibre displacement detection system is used[4] to give an accurate measurement of the amplitude of vibration.

Experimental results: Several resonances have been detected and analysed in the frequency range up to 1 MHz, and each exhibits the expected Lorentzian response of amplitude against frequency when small amplitudes of the order of nanometres are excited. The Q-factor of each resonance can be determined from the width of these curves. When the amplitude of vibration is increased, by increasing the voltage applied to the piezoelectric transducer, the response curve becomes slightly asymmetrical, and eventually develops hysteresis if the amplitude is increased sufficiently.

Fig. 2 shows an example which corresponds to the 97 kHz resonance. When the amplitude of oscillation is small, the peak of this resonance is at 97·310 kHz, but when the amplitude is increased the peak shifts towards higher frequencies. The experimental points correspond to an excited peak amplitude of 2·3 μm. If the applied frequency is increased from below resonance, the amplitude increases smoothly up to 2·3 μm and then decreases discontinuously to some negligible value at the frequency of 97·683 kHz. For decreasing frequency the amplitude-frequency relation follows the lower line, the amplitude increasing as the frequency approaches 97·310 kHz, and jumps discontinuously to the top curve at the frequency of 97·334 kHz. Further decrease in the frequency follows the top curve back down the original path.

Two different types of hysteresis, characterised by the shift of the resonance frequency, have been observed. Most of the resonances of the coupled pair of rectangular plates, as well as the resonances of the beam, shift towards higher frequencies as the amplitude of vibration is increased, but the observed resonances of the double-ended tuning fork shift towards lower frequencies.

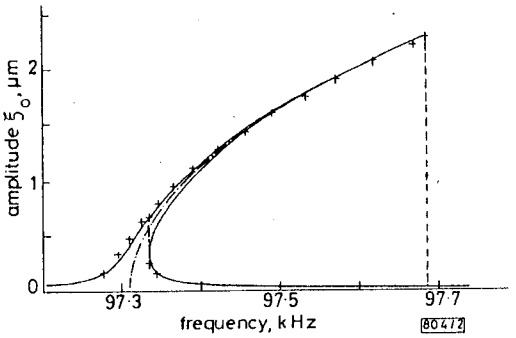

Fig. 2 *Resonance curve with hysteresis*

\+ experimental points
— theoretical curve

Theory and discussion: A single resonance of a mechanical structure can be described by the equation

$$\xi_0^2 = \frac{\xi_{0p}^2}{1 + \left(\frac{\omega - \omega_r}{h}\right)^2} \tag{1}$$

where ξ_0 is the amplitude of vibration as a function of the frequency ω, ξ_{0p} is the peak value of ξ_0 at the resonant frequency ω_r and h is a small damping coefficient.

The hysteresis behaviour described earlier can be explained in terms of a slightly anharmonic response of the vibrators.[5,6] If the restoring force R of the system is a slightly nonlinear function of the displacement ξ, e.g. let us assume a small cubic contribution, then the frequency of resonance ω_r will exhibit a small quadratic dependence on the amplitude of vibration ξ_0. Both deviations from the harmonic vibrator can be expressed in terms of a small coefficient β, as follows:

$$R = -\omega_{0r}^2(\xi + \beta\xi^3) \tag{2a}$$

$$\omega_r = \omega_{0r}(1 + \tfrac{3}{8}\beta\xi_0^2) \tag{2b}$$

where ω_{or} is the frequency of resonance when small amplitudes are excited and hence the nonlinearity of the system is negligible. If the deviation from linear behaviour is small, eqn. 1 still applies, but with ω_r being given by eqn. 2*b*.

Eqn. 2*b* shows that the shift of the experimental resonance curves towards higher or lower frequencies depends on whether β is positive or negative. A positive coefficient β corresponds to what is referred to as a hard nonlinearity and a negative β corresponds to a soft nonlinearity.

The system develops hysteresis if the shift of the frequency of resonance exceeds a certain limit fixed by the bandwidth. Eqn. 1, with ω_r given by eqn. 2*b*, becomes three-valued within a range of frequencies, and exhibits two frequencies at which $\partial\xi_0/\partial\omega$ becomes infinite, i.e. where hysteresis takes place. The relation between these frequencies and ξ_{0p} determines the minimum value of the peak amplitude required to develop hysteresis. This amplitude is given by

$$\xi_{0p}^2 > \frac{8h}{3\omega_{0r}|\beta|} \tag{3}$$

To apply this model to a particular resonance, the two parameters h and β have to be determined. The damping coefficient can be calculated by measuring the quality factor Q of the resonance when small amplitudes are excited, $Q = \omega_{0r}/2h$. The coefficient β can be determined by fitting eqn. 2*b* to a set of experimental measurements of the peak amplitude ξ_{0p} and the corresponding values of the frequency of resonance ω_{rp}, obtained by driving the piezoelectric transducer at different voltages.

The 97 kHz resonance shown in Fig. 2 exhibits a quality factor $Q = 21\,000$ and a coefficient $\beta = 1{\cdot}94 \times 10^{-3}\,\mu m^{-2}$. Taking into account these values, the theoretical curve derived from eqns. 1 and 2*b*, and plotted in Fig. 2, fits the experimental points very closely and accurately reproduces the position of the discontinuities.

The fact that different resonances and different devices can exhibit opposite types of nonlinearity shows that the nonlinear restoring force arises from the geometry of the vibrating structure and not the material.

Conclusions: The examination of the characteristics of different micromachined silicon structures for use as frequency-out sensors shows that large vibrational displacements may produce anharmonic behaviour, leading to asymmetrical resonance curves and eventually to hysteresis. These effects can restrict the use of noninterferometric interrogating techniques unless careful design of the resonator reduces the nonlinear response.

Acknowledgments: We are indebted to J. Greenwood and P. Hale of STC Technology Ltd. (Harlow) for the micromachined silicon devices and some optical fibre components, and to J. Barnett of STC Defence Systems for financial help. Acknowledgments for financial support are made by MVA to the Vicente Canada Blanch Foundation and by MJT for a CASE studentship from SERC through STC Technology Ltd. (Harlow).

M. V. ANDRES*
K. W. H. FOULDS
M. J. TUDOR

Department of Physics
University of Surrey
Guildford, Surrey GU2 5XH, United Kingdom

27th July 1987

* Departamento de Fisica Aplicada, Universidad de Valencia, Burjasot, 46100 Valencia, Spain

References

1 PITT, G. D., EXTANCE, P., NEAT, R. C., BATCHELDER, D. N., JONES, R. E., BARNETT, J. A., and PRATT, R. H.: 'Optical-fibre sensors', *IEE Proc. J, Optoelectron.*, 1985, **132**, pp. 214–248
2 DIEULESAINT, E., ROYER, D., and SERVAJAN, X.: 'Sapphire resonator', *Electron. Lett.*, 1986, **22**, pp. 266–268
3 ANDRES, M. V., FOULDS, K. W. H., and TUDOR, M. J.: 'Optical activation of a silicon vibrating sensor', *ibid.*, 1986, **22**, pp. 1097–1099
4 ANDRES, M. V., TUDOR, M. J., and FOULDS, K. W. H.: 'Analysis of an interferometric optical fibre detection technique applied to silicon vibrating sensors', *ibid.*, 1987, **23**, pp. 774–775
5 PIPPARD, A. B.: 'The physics of vibration' (CUP, Cambridge, 1978, Vol. 1)
6 DINCA, F., and TEODOSIU, C.: 'Nonlinear and random vibrations' (Academic Press, New York, 1973)

LONG-WAVELENGTH PINFET RECEIVER OEIC ON A GaAs-ON-InP HETEROSTRUCTURE

Indexing terms: Optoelectronics, Optical receivers

A long-wavelength PINFET OEIC has been fabricated on a GaAs-on-InP heterostructure for the first time. A receiver sensitivity as high as −31 dBm for 600 Mbit/s NRZ has been obtained. The great potential of the GaAs-on-InP heterostructure for high-performance, long-wavelength OEIC applications has been demonstrated.

Introduction: The scope of optical fibre communications applications has expanded greatly from trunk line systems to subscriber systems. The long-wavelength InP-based optoelectronic integrated circuit (OEIC) with high performance and high reliability is one of the most important key elements for such new systems.[1] InP-based OEICs, however, are still in the preliminary stage, in spite of their importance, due to the immaturity of InP-based electronic circuit technology.

The strained heteroepitaxial GaAs–InP structure is an attractive approach. This kind of structure has great potential for combining GaInAs(P)/InP long-wavelength optical components and the mature GaAs integrated circuit technologies. There have been several reports on fabricated InP-based materials grown on GaAs substrate (InP-on-GaAs structure).[2–4] The InP-on-GaAs structure, however, involves a problem with regard to lattice mismatch between the InP-based optical components and the GaAs substrate. There is apprehension that the performance and reliability for minority-carrier devices, such as photodiodes and especially laser diodes, might deteriorate due to the lattice mismatch.

This letter proposes a new kind of heteroepitaxial structure: the GaAs-on-InP structure. This structure makes possible long-wavelength optical component integration on an InP substrate with perfect lattice matching. The GaAs electronic circuit is formed in the strained heteroepitaxial GaAs layers on the Inp substrate. The device performance and reliability for majority-carrier devices, such as FETs, are hardly affected by the lattice mismatch. The first OEIC fabricated from the GaAs-on-InP structure is described.

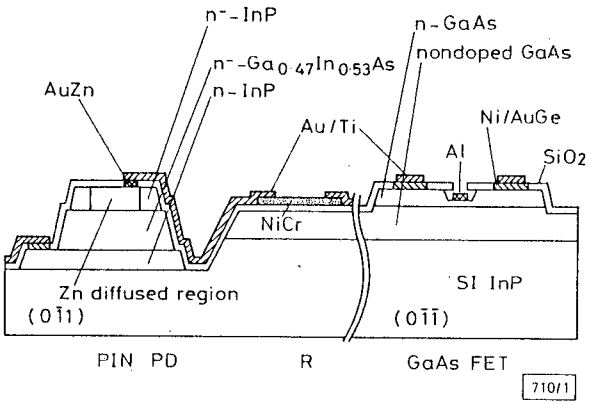

Fig. 1 *Cross-section of long-wavelength PINFET OEIC fabricated on a GaAs-on-InP heterostructure*

Fabrication: Fig. 1 shows a cross-section of a receiver OEIC. The GaAs-on-InP structure wafer was prepared by a combination of VPE and MBE. First, GaInAs/InP PIN photodiode layers were grown on a stepped substrate by conventional VPE. The photodiode layers consisted of a 0·5 μm-thick ($n \simeq 5 \times 10^{15}\,cm^{-3}$) InP window layer, a 2 μm-thick ($n \simeq 5 \times 10^{15}\,cm^{-3}$) GaInAs absorbing layer and a 1 μm-thick ($n \simeq 5 \times 10^{17}\,cm^{-3}$) InP contact layer. After the wafer was preferentially mesa-etched, to form the PIN photodiode on the bottom part of the step-formed substrate, a 0·5 μm-thick undoped GaAs buffer layer and a 0·3 μm-thick Si-doped ($n \simeq 2 \times 10^{17}\,cm^{-3}$) GaAs channel layer were successively grown by strained heteroepitaxy by MBE at a 500°C substrate temperature.[5,6] Finally, the GaAs layers were preferentially mesa-etched to form a GaAs MESFET on the upper part of the stepped substrate.

The receiver OEIC was fabricated by a conventional OEIC process.[1] After a planar PIN photodiode had been formed by selective Zn diffusion, the photodiode *p*-electrode was formed by Au–Zn and the photodiode *n*-electrode, MESFET source and MESFET drain were formed by Ni/Au–Ge, using the lift-off technique. The Al gate electrode was formed by a conventional recess gate process. Load resistances were also integrated monolithically by Ni–Cr evaporation.

Device performance: Fig. 2 shows a photograph of the chip and a circuit diagram for the fabricated receiver OEIC. A GaInAs PIN photodiode, GaAs MESFET and two load resistances were monolithically integrated. The chip size is 500 × 700 μm. The PIN photodiode photosensitive area is 60 μm in diameter. The FET gate length and gate width are 1·8 μm and 280 μm, respectively. The PIN photodiode load resistance and FET load resistance are 3·8 kΩ and 570 Ω, respectively.

The dark current characteristics for the integrated GaInAs PIN photodiode were measured. At <5 V reverse bias the